REPORT DOCUMENTATION PAGE

Form Approved
OMB NO. 0704-0188

1. AGENCY USE ONLY (Leave Blank)	2. REPORT DATE 31 March 2003	3. REPORT TYPE AND DATES COVERED Final 1 June 2000 – 31 May 2003

4. TITLE AND SUBTITLE
Spectrally Analyzed Embedded Infrared Fiber Optic Diagnostic of Advanced Composite Propellant Combustion

5. FUNDING NUMBERS
DAAD19-00-C-0095

6. AUTHOR(S)
Joda Wormhoudt

7. PERFORMING ORGANIZATION NAME(S) AND ADDRESS(ES)
Aerodyne Research, Inc.
45 Manning Road
Billerica, MA 01821-3976

8. PERFORMING ORGANIZATION REPORT NUMBER
ARI-RR-1368

9. SPONSORING / MONITORING AGENCY NAME(S) AND ADDRESS(ES)
U. S. Army Research Office
P.O. Box 12211
Research Triangle Park, NC 27709-2211

10. SPONSORING / MONITORING AGENCY REPORT NUMBER
41260.1-CH

11. SUPPLEMENTARY NOTES
The views, opinions and/or findings contained in this report are those of the author(s) and should not be construed as an official Department of the Army position, policy or decision, unless so designated by other documentation.

12 a. DISTRIBUTION / AVAILABILITY STATEMENT
Approved for public release; distribution unlimited.

12 b. DISTRIBUTION CODE

13. ABSTRACT (Maximum 200 words)

This is the final report for a program to extend an embedded-infrared-fiber propellant strand burning diagnostic by replacing bandpass filter detection by spectral detection. This work builds on previous investigations into the chemical and physical processes occurring in the condensed phases of nitramine advanced composite propellants, in which we observed decomposition product gases by infrared absorption in a small volume below the flame front. Detection of infrared absorption spectra along with video camera and embedded thermocouple records allows characterization of the evolution of decomposition regions by correlating time, spatial location, temperature and decomposition species fractions. Much of the effort of the program went into optimizing the sensitivity of the FTIR spectrometer/fiber optic apparatus, and into constructing test articles. The difficulty of these tasks limited us to only a handful of successful burns. The spectra obtained clearly show N_2O and CO_2, thus confirming our earlier work and adding a new species to those detected previously. Evidence for other gases is less certain.

14. SUBJECT TERMS	15. NUMBER OF PAGES
solid propellant combustion infrared fiber optic absorption diagnostic	32
	16. PRICE CODE

17. SECURITY CLASSIFICATION OR REPORT	18. SECURITY CLASSIFICATION ON THIS PAGE	19. SECURITY CLASSIFICATION OF ABSTRACT	20. LIMITATION OF ABSTRACT
UNCLASSIFIED	**UNCLASSIFIED**	**UNCLASSIFIED**	**UL**

NSN 7540-01-280-5500
(Rev.2-89)
by ANSI Std. 239-18

Standard Form 298
Prescribed
298-102

Table of Contents

List of Figures

1. Introduction

This is the final report for a program by Aerodyne Research, Inc. (ARI) to obtain data on the chemical and physical processes occurring in the condensed phases of nitramine and other advanced composite propellants in strand burning experiments. This work builds on the embedded fiber optic diagnostic work carried out at ARI from 1993 to 1996. However, instead of using individual spectroscopic bands and detecting only one or two species as was done in that earlier work, our goal in the present program was to investigate the feasibility of spectral detection, which could in principle allow the simultaneous detection of most of the major infrared-active species.

Embedded fiber optics are currently the only method of monitoring condensed phase decomposition products in burning propellants, allowing confirmation of measurements currently being made in a variety of laboratory experiments. All of these experiments will support the development of first-principles models of condensed phase processes, just as a much more extensive program of *in situ* diagnostics and laboratory experiments has led to more advanced models of the gas phase processes in the dark zone and secondary flame. Furthermore, it now appears that *in situ* diagnostics of the primary flame zone under realistic conditions will not be possible. However, embedded fiber diagnostics of the input species to that zone are possible, leading to the conclusion that the only way to characterize the primary flame zone may be to combine diagnostics in the condensed phase with gas phase and gas/surface modeling.

The statement of work for the program began with a task to upgrade the existing high pressure strand burner/fiber optic absorption apparatus by interfacing it with an available Fourier transform infrared (FTIR) spectrometer. Propellant strand burning experiments would then be made in which the absorption due to gas phase decomposition products was monitored in an observation volume inside the strand. Temperature measurements using embedded thermocouples and video records leading to burn rates would also be made, as they had in the previous, bandpass-filter experiments. Once the principle had been demonstrated, it was hoped that further observations at higher data rates could be made using either a fast-scanning FTIR spectrometer or an infrared diode array spectrometer.

When this program was first proposed in 1996, linear InSb detector arrays had become available that seemed to promise detection over the entire infrared region of interest with time resolution and sensitivity comparable to our single detector, bandpass filter instrumentation. We believed that this improvement in array capabilities would continue, but in fact by the time our program began in June of 2000, the only commercially available arrays were two-dimensional arrays with costs and capabilities entirely inappropriate for the application we proposed. This led to the plan described above, to begin using an FTIR spectrometer currently available at

Aerodyne, which we thought would be sensitive enough, and might be fast enough. If experiment showed that it could not be both fast enough and sensitive enough, we planned to move on to one of two alternatives. On one hand, we thought we had identified a faster FTIR spectrometer we could rent. On the other hand, we knew of a line of inexpensive array detectors that were faster but less sensitive than the ARI FTIR with which we would begin (so this choice would only be of interest if we could improve the infrared power transmitted through the fibers).

It became clear that a less sensitive detector would not be usable, so the second alternative was never investigated. We did investigate two faster FTIR instruments, but concluded they would also not be sensitive enough for this application, as we will describe in somewhat more detail below. Therefore, the main focus of this report will be on the experiments performed using the MIDAC 2400-C FTIR owned by ARI. To put those observations in context, we will first review the earlier bandpass filter observations.

2. Previous Work Using Bandpass Filters

Our earlier work on an embedded infrared fiber optics condensed phase diagnostic of burning propellant strands was funded over 4 years under ARO Contract Numbers DAAL03-91-C-0008 and DAAH04-93-C-0053. A high pressure strand burner was constructed, and a series of experimental configurations was investigated. By the third year of the program, a particularly promising technique had been identified, involving the detection of gaseous decomposition products evolved into an observation volume whose observation path length was a substantial fraction of the strand diameter. Then, a series of experiments was carried out observing the appearance of the nitramine decomposition products N_2O, NO_2, and NO. These experiments were documented in two Combustion and Flame papers.[1-2] These results, when correlated with simultaneous observations of embedded thermocouple temperatures and video images of the burning strand, suggested hypotheses for the physical and chemical nature of the condensed phases of the propellant near the burning surface.

The basic experiment involved creating a small void inside a strand of propellant, whose gaseous contents are measured by infrared and/or visible absorption using a pair of fluoride glass optical fibers at each end of the void. We observed changes in transmission through this observation volume, as well as temperatures from thermocouples embedded near it in the same axial plane of the strand. The transmission and temperature records were correlated with the video record of flame front position.

Figure 1 shows the high pressure strand burner, propellant strand, and fiber optics. The strand burner is a copy of a device in use at the U. S. Army Research Laboratory, Aberdeen Proving Ground, with some modifications to accommodate fiber optics. The only propellant observed was XM39, composed of 75% RDX and 25% binder. Experiments were performed at two pressures, 1 and 6 atm. XM39 will not burn in an inert atmosphere at 1 atm, so we used secondary combustion of the gaseous decomposition products with air to support the primary combustion of the solid propellant. A combination of nitrogen addition to the air and a large enough flow velocity around the strand were used to prevent burning down the side of the strand. Under these gas flow conditions, the strand burns with a roughly flat melt layer and a slightly concave burning surface.

A schematic diagram of the optical components of the bandpass filter experiment is given in Figure 2, which shows the apparatus in its configuration for the simultaneous measurement of N_2O and NO_2. The mirrored tuning fork chopper modulated both the infrared source (a globar) and the red and green HeNe lasers, and so their transmitted signals, at 1200 Hz. The embedded optical fibers pass through the baseplate of the strand burner (by means of SMA connectors), as do thermocouple wires and leads connecting a variac to a V-shaped segment of nichrome wire

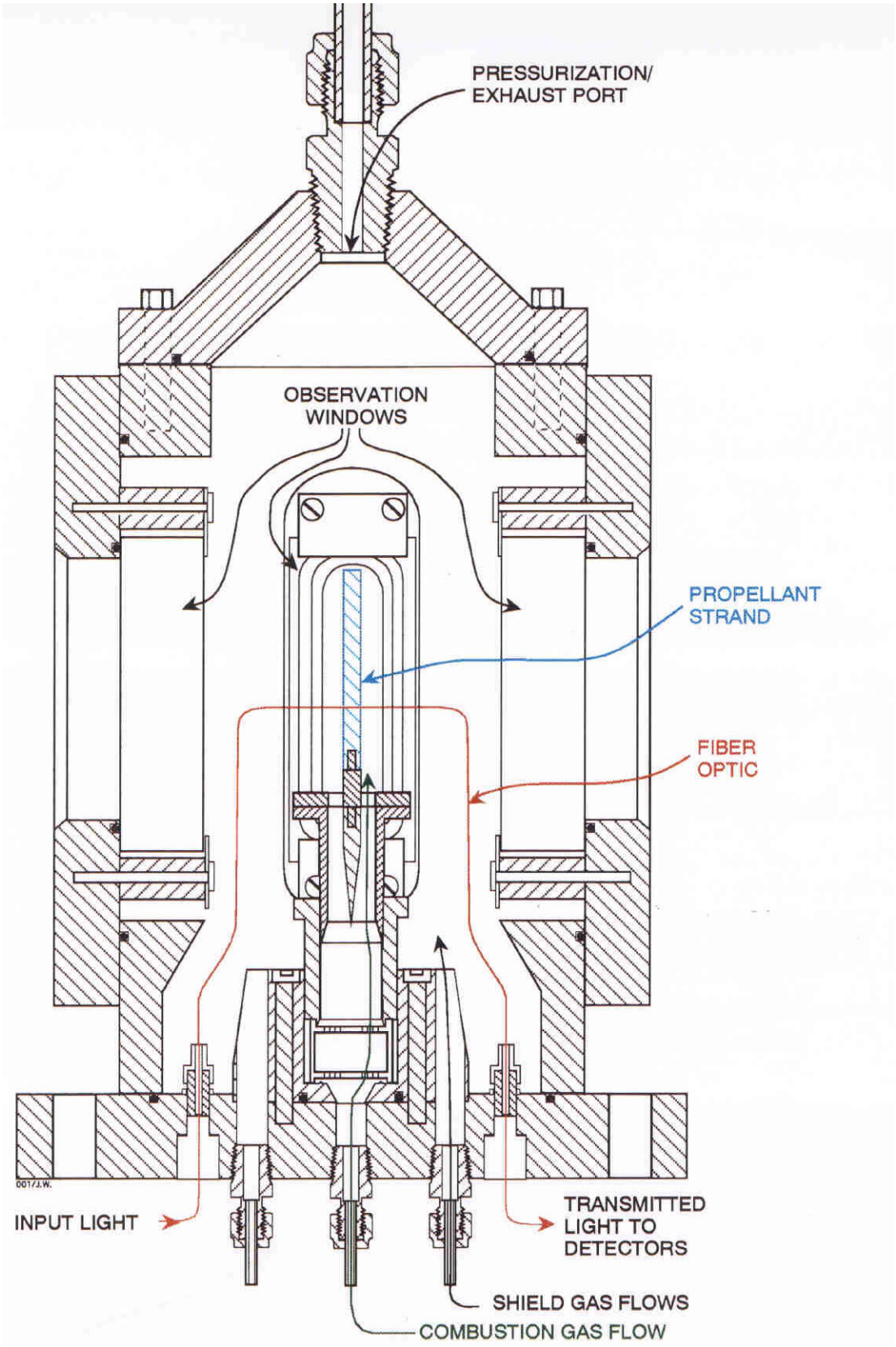

Figure 1. Cross-Section of Strand Burner, Propellant Strand, and Embedded Fiber Optics

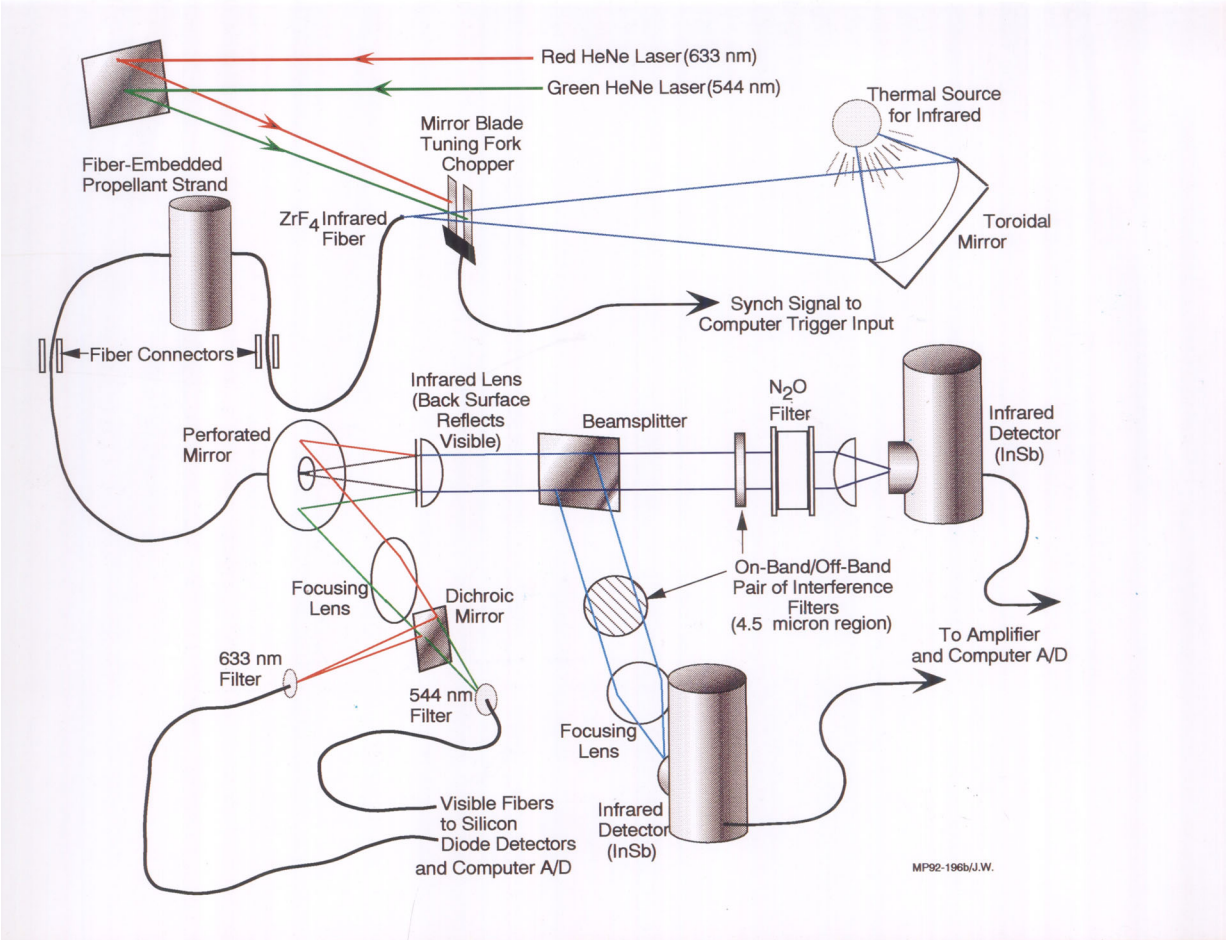

Figure 2. Schematic Drawing of Fiber Optic Absorption Experiment. In this configuration, N2O was detected using pairs of infrared bandpass filters and infrared detectors, and NO2 by the differential absorption of red and green HeNe lasers.

pressed against the top of the strand to provide ignition. The gaps between the source and detector fibers were in the 0.2 to 0.5 cm range. Infrared light collected by the fiber on the detector side was divided by a 50/50 beamsplitter and passed through a pair of narrow band infrared interference filters before being focused onto InSb infrared detectors. The visible light from the two HeNe lasers was reflected from the infrared lens and separated

A data acquisition computer read a signal point from each infrared and visible detector at each on and off point of the chopper. Computer data acquisition for each chopper cycle was triggered by the synchronization signal from the commercial chopper controller. In addition to detector signals, the computer read embedded thermocouple temperatures at a 30 Hz rate. A high-resolution video system was used to record each burn. The beginning of data collection

was accompanied by a computer signal to the video recorder which starts its time clock. The video record of each burn was examined to yield a record of the position of the burning surface, synchronized with the computer records of infrared transmission and thermocouple temperatures.

In our one experiment involving simultaneous measurement of NO_2 and NO, a tunable infrared diode laser spectrometer system was used to scan across a single NO absorption line. To allow optical access to the input fiber for the diode laser beam and the two HeNe beams, it was necessary to remove the thermal source and dispense with the N_2O measurement. One of the two infrared detectors shown in Figure 2 was used to detect the diode laser signal after passage through the strand (the infrared beamsplitter, bandpass filter, and N_2O filter cell were all removed for this experiment). The diode laser was effectively modulated by rapidly (1500 Hz) sweeping its frequency across the selected spectral interval, so no mechanical modulation was needed. Therefore, a small mirror (past which the diode laser beam could pass to the input fiber) was placed at the position of the tuning fork chopper in Figure 2, and a wheel chopper was used to mechanically modulate the two HeNe beams. A second computer controlled the diode laser scan and acquired its absorption spectra, beginning upon a synchronization signal from the computer which dealt with the visible detectors, thermocouples, and video recorder.

The characteristic of our diagnostic technique that caused us to choose it over other possible implementations of fiber optics is that direct absorption measurements over a defined path are an absolute, quantitative measurement of the gas concentrations in the measurement volume. There are, of course, several sources of uncertainty in the parameters required to make these quantitative measurements. Still, infrared band strengths are known molecular constants, tabulated in the literature, and we can put reasonable limits on the uncertainties in our experiments, so that error limits of only 20-30 per cent in concentrations are certainly achievable.

In N_2O detection using bandpass filters, the filter responses were calibrated computationally, using Fourier transform infrared spectrometer measurements of the bandpass filter transmission curves, and N_2O spectral absorbance values derived from the HITRAN absorption line database[3]. The transmitted intensity signals were obtained from computer files of the detector outputs by differencing each pair of chopper-open and chopper-closed values. These intensity records were then averaged; depending on the signal to noise level, averaging times were used which yield data streams at rates from 60 to 5 Hz. After the fiber burned through, the remaining data stream was averaged to give a zero level which is subtracted from each detector signal before their ratio is taken. The value of this ratio, relative to its value before ignition, gave a fractional transmission in the N_2O band which was compared with the calibrations described above to yield column densities. Since we were always comparing transmission at a molecular absorption peak to that in a nearby spectral region with lower absorption, changes in

transmission due to misalignment of fibers and other causes without a spectral dependence were self-calibrating and did not result in spurious data.

Figures 3 gives an example of the data traces near the time of decomposition gas appearance for the most observed species, N_2O. In the solid curve we see the ratio of the intensity from the N_2O-sensitive detector to that from the detector observing the nearby reference band. This ratio is proportional to transmission in the N_2O band. We can note that at 15.09 seconds, the individual intensities have already dropped by one-third while their ratio has dropped by only 10 per cent. This corresponds to an N_2O absorbance only one-tenth of the value at 15.11 seconds. The observation that transmitted intensity begins to drop even before any decomposition gas absorption is detected is a general one. Indeed, in the most unfortunate cases, all transmitted light was lost before any N_2O was detected.

Although in this example there is a slow decrease in the ratio between 15.06 and 15.10 seconds, in many other observations there is essentially no change in the ratio (even as the individual intensities each

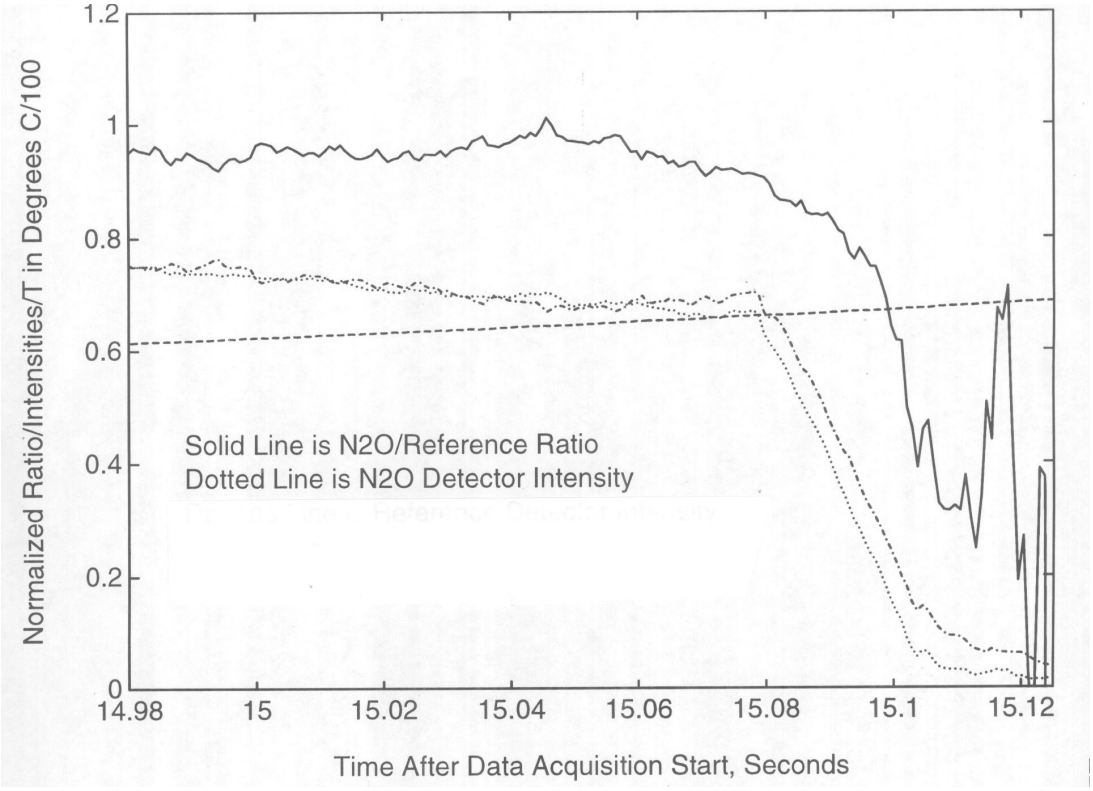

Figure 3. Bandpass Filter Observation of N2O in XM39 Strand Burning at 6 atm Pressure.

drop by an order of magnitude) until a sudden drop signals the appearance of a substantial column density of N_2O. This abrupt appearance, here reaching a fairly constant level in only a few 60 Hz data points, was seen in almost all 6 atm experiments, while in most 1 atm experiments N_2O appeared more gradually. If we assume that the N_2O is at the temperature of the embedded thermocouples we can use the known absorption path length to calculate an N_2O mole fraction of about 0.1 for this case. In other experiments the N_2O mole fractions observed ranged from 0.05 to 0.24, similar to values seen by other workers for pure decomposition gases from RDX.

After its initial abrupt appearance, the N_2O level (and the infrared transmission through the observation volume) is maintained for only a few data points (about 0.01 seconds). In earlier observations, longer steady state times were seen, with an average of about 0.4 s in 6 atm cases and for between 1 and 2 s in 1 atm cases. After this steady state time, the transmitted intensities have dropped enough that their ratio no longer carries useful information. The individual intensity traces have been plotted before the corrections to their true zero values were applied, so it is difficult to tell from the figure if both bandpass intensities, or only one, have decreased to the S/N<1 level. However, some experiments were clearly concluded by events whose effects on the transmission had no spectral dependence over the range of the bandpass filters, such as misalignment of the fibers or entry of some liquid phase into the observation path.

The dashed line in Figure 3 denotes the temperature of the embedded thermocouple. It can be seen that the appearance of the N_2O takes place while the observation region is at a temperature of somewhat under 70 °C, consistent with the temperature range of 35-155 °C for all 6 atm cases. The value of fiber insertion plane to burning surface distance at the time of N_2O appearance (0.1 cm) for this case is also representative of the range (0.15 ± 0.11 cm) seen in all cases.

In other experiments we used the intensity traces for the two visible HeNe lasers to derive peak NO_2 mole fractions from 0.05 to 0.15, in the range expected for pure decomposition gas. NO_2 appearance often significantly preceded that of N_2O, and was much less abrupt. We were only able to carry out one experiment using a tunable diode laser to monitor NO simultaneously with the visible absorption detection of NO_2. The transmission at the peak of the NO spectral feature exhibited similar characteristics to the N_2O curve in Figure 3: an abrupt appearance of a large mole fraction (in the 0.20-0.25 range) when the burning surface was about 0.1 cm from the observation region. Meanwhile, the NO_2 transmission curve in this experiment had the characteristics noted above, showing NO_2 appearance almost 2 seconds before NO, with a much more gradual evolution into the observation volume. Furthermore, in this case, the NO_2 seemed to substantially disappear before the visible transmission was lost. This phenomenon, also observed for N_2O in two cases where transmission was maintained through the observation

region even though it attained particularly high temperatures, may be attributable to reactions with the walls of the observation volume.

Our bandpass filter work produced several major results. We observed N_2O, NO_2, and NO, gaseous decomposition products of RDX, evolving into a small volume in the condensed phase of a burning nitramine propellant strand. As we will discuss below, this result is expected, in that it is consistent with other observations of the chemistry of RDX decomposition. A second result is that many cases show an abrupt N_2O evolution at a time when the propellant forming the observation volume is still at a temperature well below that needed to produce rapid decomposition of RDX. This observation by itself will of course not fully specify the microstructure of the burning strand and the physical mechanisms which lie behind it, but it leads us to the speculation that the suddenly appearing N_2O originates in pressurized bubbles inside liquid RDX which in turn is contained inside a matrix formed by the propellant binder. This matrix would have to be structurally sound enough that some bubbles are prevented from releasing their contents upward into the flame region, but instead eject decomposition gas into the observation volume when cracks open up into it. A third result is the different time behavior of NO_2 appearance compared to those of N_2O and NO, a difference which may carry information about differences in chemical mechanisms of formation of these species.

In order to appreciate the full significance of our spectroscopic results, it is necessary to correlate them with the information in the embedded thermocouple records, an example of which is shown in Figure 4. A schematic of average or representative versions of such plots and the positions of other important events is given in Figure 5. The temperature record in Figure 4 is similar to that in Figure 3, but replotted on a semilog scale as a temperature difference from ambient. In this plot, the thermal wave into an inert propellant will be a straight line, since the temperature gradient is an exponential with a scale length related to the ratio of the thermal diffusivity of the propellant and its burning rate.[4] A change in slope with

continued exponential behavior, such as at the point in Figure 4 marked "change in α", may be associated with a change in the physical properties of the propellant in the absence of an ongoing chemical change, such as a change in the thermal conductivity (α) due to the appearance of cracks or voids in the solid. A deviation from exponential behavior, on the other hand, such as the one marked "inflection point", denotes a chemical, heat-releasing or heat-consuming step. If the result is that the temperature gradient is shallower (extends further into the condensed phase), as we see above the upper transition point in Figure 4, this indicates heat release. In simple propellants this point indicated the position of the flame front, but in this composite propellant we believe it to be associated with the onset of RDX decomposition. The temperature at the upper transition point marked in Figure 4 is somewhat below 200°C, while we expect burning surface temperatures to be more around 400°C. That temperature is reached at the point where the temperature gradient

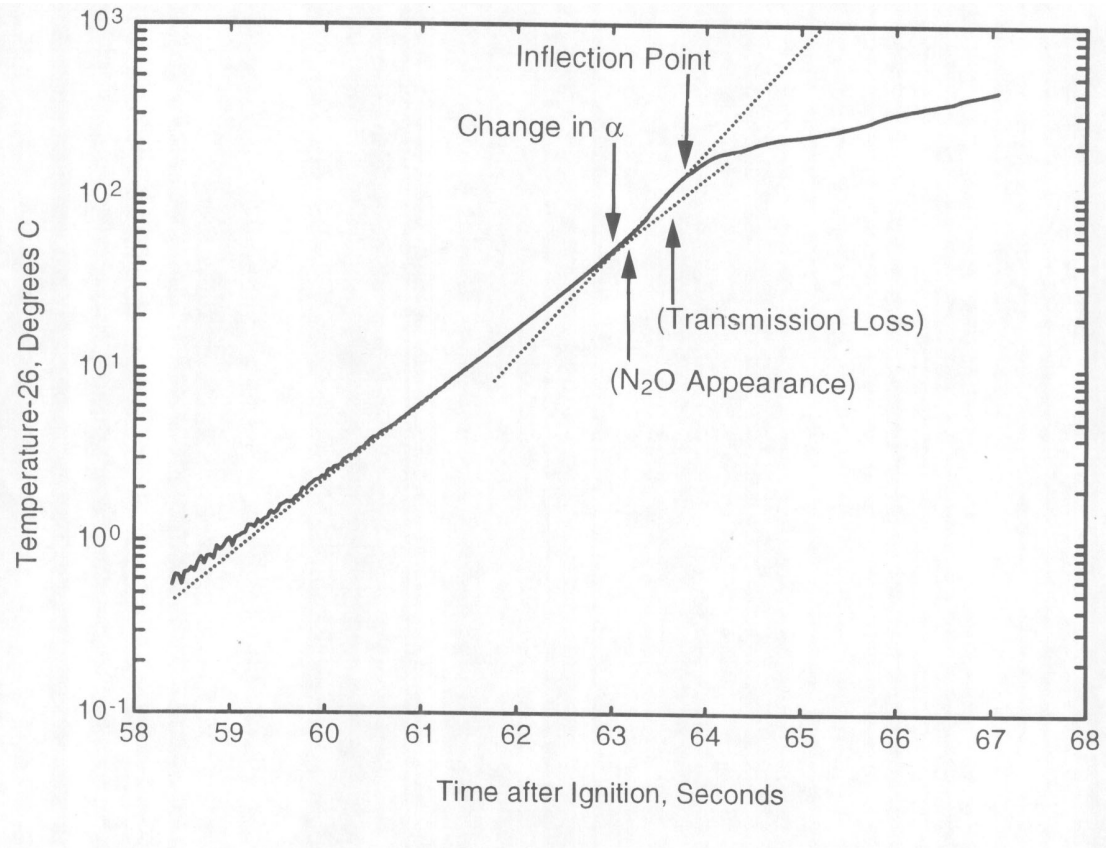

Figure 4. Typical Observed Thermal Wave for 6 atm Burning of XM-39 Strand

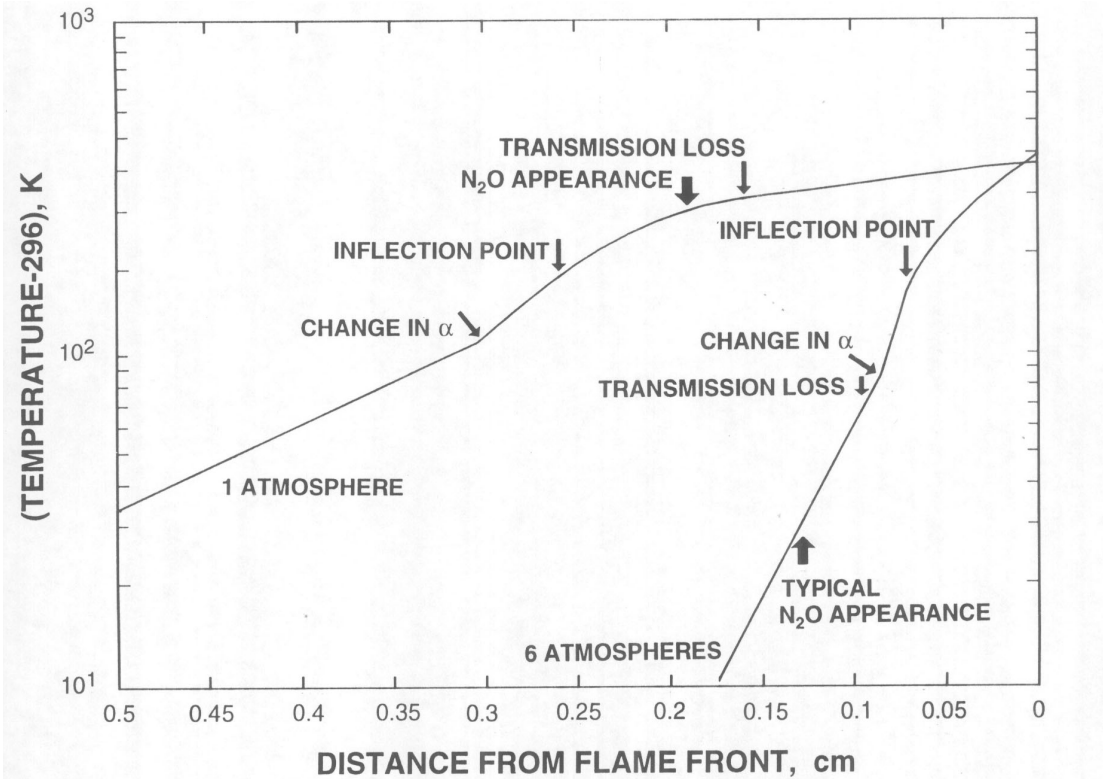

Figure 5. Qualitative Sketch of Typical Thermal Waves and Positions of Other Events in Strand Burning Observations.

flattens out, consistent with passage of the thermocouple into the gas phase. It turns out that this point has not yet been reached when the flame front has reached the fiber plane by the video record. This indicates the level of uncertainty of burning surface position measurement due to the slightly cupped surface. In many cases only the edge of the strand could be seen in the video image.

It is of interest to examine the event positions marked in Figure 5, which represent the most typical sequences of events observed at the fiber insertion plane. The sequence is seen to be different at the two pressures. At 1 atm, both temperature transition points can arrive first, followed in fairly rapid succession by the appearance of N_2O and the loss of transmission, with the arrival of the flame front occurring considerably later. At 6 atm, the N_2O appears first, substantially before the arrival of either temperature inflection point, and therefore in a lower temperature regime. Loss of transmission, upper transition point arrival, and arrival of the flame front region all occur at about the same time.

It can be seen that the two temperature history transition points occur in the same temperature ranges for the two pressures, leading us to suggest that they are due to physical or chemical changes in specific propellant ingredients. The point of appearance of N_2O, on the other hand, is not at all correlated with temperature at the observation point. Instead, the N_2O appearance point is much better correlated with a particular flame-to-fiber distance, around 0.2 cm, than it is with the local temperature. This suggests the speculation that the cracks which suddenly release bursts of pressurized decomposition gas into the observation region can propagate only distances of this order in this propellant. The fact that decomposition gas can travel these relatively large distances, however, is the basis for the fortunate circumstance that our observations in cool, structurally sound solid propellant nevertheless monitored a region nearer the flame front in which RDX has melted and is releasing decomposition products. The appearance of large mole fractions of those gases in such an abrupt manner (NO_2 excepted) and the large volume of our observation region (200 μm diameter by 3000 μm length) compared to the small size of bubbles in the true liquid or melt layer (constrained in diameter to less than or equal to its thickness of order 300 μm) suggested a further speculation: that the reservoirs of decomposition gas which eventually fill our observation volume when cracks connect the two regions must be substantially pressurized. This suggestion, while not new, has an important corollary: bubbles within the melt layer cannot support high over pressures without simply bursting upward into the gas phase, so that if pressurized voids are involved they must be instead in a layer of the propellant containing both liquid RDX (since RDX must melt before its decomposition rates are appreciable) and a binder matrix of some remaining structural soundness. In the case of XM39, whose major binder component has a substantially higher melting point than RDX, this is plausible, even setting aside the fact that melting will not be an instantaneous event. It is for these reasons that we have

suggested that this technique may be most successful for a restricted class of composite propellants. Still, some very important and well studied formulations are members of this class, so we expected that these techniques should be able to produce a very substantial set of useful observations without further basic technical evolution.

Slow filling, seen for N_2O at one atmosphere pressure, seems to be the rule for NO_2 even at 6 atm. We interpreted this to mean that NO_2 is formed in a region nearer to the observation volume than the region which delivers pressurized decomposition gases in an abrupt filling event. These nearer regions would already be connected to the observation volume through existing cracks and connected voids in the composite propellant, so gas might simply effuse into the observation region as it was formed. This could be expected for N_2O at 1 atm because under these low burning rate conditions the thermal wave reaches further into the propellant, and regions in which RDX can melt will be closer to the observation volume (and will remain close but not coincident for a longer time than in the faster-burning 6 atm case). For NO_2, we conclude that its slower filling rate sends the same message as the observation that it can substantially precede the appearance of either N_2O or NO: in strand burning, that it is formed in regions directly connected to the observation region, before substantial amounts of the other two gases are produced.

In summary, we drew two major conclusions from our bandpass filter work: N_2O, NO_2, and NO are all observed as decomposition products of RDX embedded in binder under actual combustion conditions, and they are formed in high temperature regions of the condensed phase but are able to penetrate through cracks into regions of the propellant which are otherwise little affected by the advancing flame front. Of course, our observations by themselves will not fully specify the structure of a burning strand near the burning surface and the physical mechanisms which shape it, but they certainly strongly encourage the speculation that the suddenly appearing decomposition gases originate in pressurized bubbles inside liquid RDX which in turn is contained inside a still solid matrix formed by the propellant binder. This matrix would have to be structurally sound enough that some bubbles are prevented from releasing their contents upward into the flame region, but instead eject decomposition gas into the observation volume when cracks open up into it.

3. New Apparatus and Experimental Results

In principle, the apparatus used in this program, depicted in Figure 6, differs from that used in our earlier work only in detecting full infrared spectra rather than measuring intensities in a few bandpasses. Infrared fibers are still inserted into drilled holes in propellant strands, and now carry light from an FTIR spectrometer to an infrared detector. Infrared absorption measurements are still made in a 0.3 cm gap between the pair of fibers in the center of the strand. The goal is still the combination of infrared absorption measurements along with video camera and embedded thermocouple records to characterize the evolution of decomposition regions by correlating time, spatial location, temperature and decomposition species fractions.

However, in practice there were several major changes to the apparatus, and new challenges to be overcome before good spectra could be obtained. We will begin by reviewing the changes to the apparatus, then present example data from one burn as well as averaged data from all successful burns. We conclude with a discussion of how our observations could be put in the context provided by current models and our earlier experimental work.

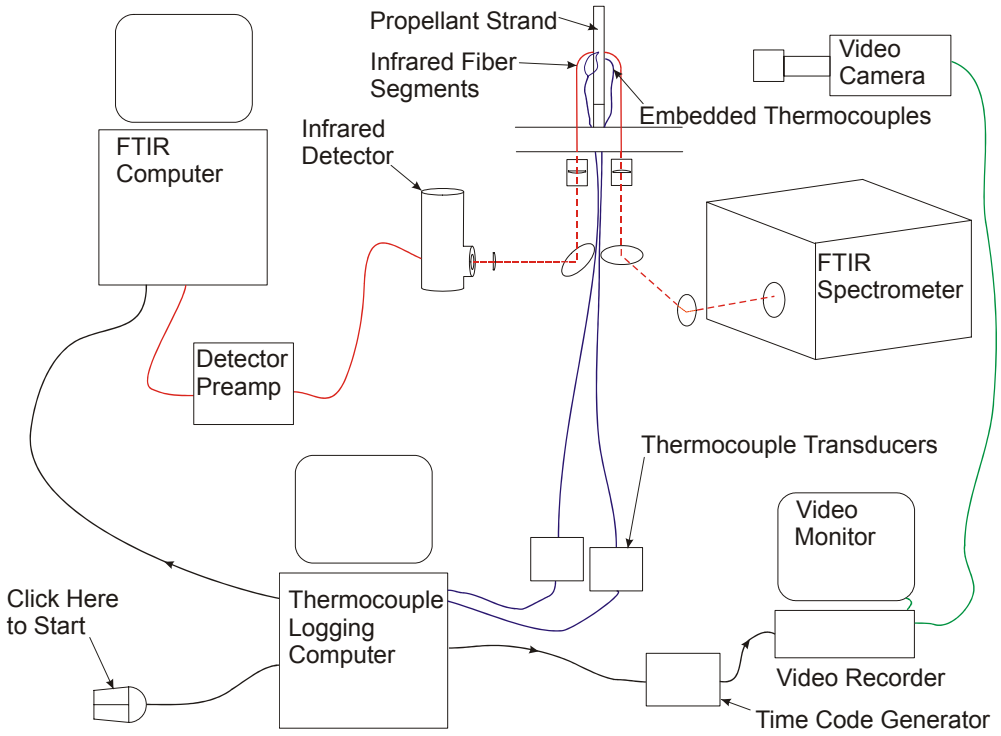

Figure 6. Schematic Diagram of Apparatus Used in the Present Program, Utilizing an FTIR Spectrometer for Spectrally Analyzed Embedded Fiber Diagnostics of Strand Burning.

3.1 Apparatus Description

As part of the work of apparatus reassembly, several components were upgraded. Particular examples include changing to infrared fiber from a new and better source, writing a new Windows-based data acquisition program to replace the previous DOS program (including synchronized triggering for the spectrometer as well as video and thermocouple data), and developing an all-new optical train to carry the infrared light between the fibers and the spectrometer and detector. We will discuss each in turn.

In our previous work, our supplier of fluoride glass optical fibers was only able to sell us whatever remainders of custom orders happened to be available. This meant that the specifications of each new order of fiber were different. Now, the fiber we use is a Thorlabs catalog item (0.28 NA, 150 μm core diameter , 0.5 to 4 μm transmission from KDD Fiberlabs), so although we still find our orders being assembled from several production lots, the key parameters can be counted on as constants. In particular, the fact that we can rely on the outer diameter of the fiber remaining constant led us to change our philosophy on mating fibers to fiber connectors. In past work, we had fiber connectors with holes accommodating only the actual glass fibers, requiring that we strip off all the cladding layers before inserting the fiber into the connector. In this program, we drilled the connectors to match the outer diameter of the clad fiber, and so could mount fibers in connectors (using hot-melt glue) without stripping them. On the other hand, stripping is still required for the fiber ends inserted into the propellant strand (we want the fiber to be the least perturbation possible) and we have found the new fiber to be more resistant to stripping. Assembly of fiber segments and fully instrumented strands continued to be a major challenge.

The data acquisition program used in our previous work had the task of reading the outputs of several detectors (infrared and visible) as well as the temperatures of the embedded thermocouples. In the current program, the infrared detectors were replaced by an FTIR spectrometer, operated by its own computer. It made sense to write a new software package that could still read multiple A/D inputs at specified rates and record an ASCII file of times and voltages, but could also send a variety of triggering pulses so that at the same time it began to write its own data file, other synchronized recording could begin. In the experiments reported here, there were two such triggering pulses. One, as in previous work, started the time code generator, so that the (already recording) video record had a clock whose start time was synchronized with the ASCII file of thermocouple temperatures. The other pulse started the FTIR spectrometer, whose spectral files also have an elapsed time written in them. The FTIR spectrometer is operated by a commercial software package, and we considered a number of ways to interface the triggering/data acquisition computer to it before deciding that the most straightforward solution was a mouse with two tails. This mouse was used to position the FTIR computer's cursor over the "start scanning" button in the FTIR user interface, and the "second

tail" of the mouse was a cable leading to the D/A port of the triggering computer that was to give the FTIR trigger pulse. This pulse and the modified circuitry in the two-tailed mouse resulted in the FTIR software receiving a "mouse click" that was precisely synchronized with the starts of the other data records. The entire software package operated very reliably, once we understood a few pitfalls that initially caused the loss of data for a few burns (for instance, once the FTIR cursor is positioned, it's safest to tape the mouse down so it can't move).

The optical system shown in Figure 6, though straightforward enough, was the product of considerable evolution during the program. It includes three flat steering mirrors to connect the FTIR spectrometer with the input fiber and to connect the output fiber with the infrared detector, and three lenses. The first lens focuses the (approximately collimated) infrared light from the FTIR onto the input fiber. The FTIR has an infrared source inside it, whose light is then modulated by the moving mirror in this Michelson-design spectrometer. The second lens then approximately collimates the light emerging from the output fiber. Finally, the third lens focuses the infrared beam onto the face of the infrared detector. At present, all three lenses are 5 cm focal length, 1 inch diameter barium fluoride lenses. These have the advantage of passing visible light, so that the optical system can be aligned using a HeNe laser input into the fibers.

Propellant strands burned in this program were the same formulation we used in our earlier observations, XM39. This nitramine composite propellant is 76 per cent RDX with most of the balance made up by the binder cellulose acetate butyrate and the plasticizer acetyl triethyl citrate. Burning conditions were also the same as in our earlier work, burning at 6 atm pressure, in air with added nitrogen for a flat burning surface. The operation of the apparatus began with the sealing up of the strand burner, turning on of the exhaust blower, and the setting of gas flows and burner pressure. Then the video recorder was started, followed by ignition of the propellant strand using a hot filament. A strand segment around two inches in length could burn long enough that its burning surface became flat and perpendicular to the strand axis (and the flow of gas around the strand). When the burning surface was within roughly a half inch of the fiber plane, the FTIR spectrometer and thermocouple data acquisition computers were triggered. After the burn, the ASCII files of thermocouple temperatures could be plotted directly. The video record could be replayed frame by frame with occasional ruler measurements to generate a small file of flame front positions. Software routines allow the FTIR file containing the entire set of spectra (recorded at about 14 Hz) to be excerpted as a file containing all those spectra of interest, which is then broken into individual spectra that can be plotted and analyzed.

3.2 Model Spectra

Our goal was to detect most of the major nitramine composite propellant decomposition gases, and the sequence of their arrival in the observation volume near the burning surface. In the proposal for this program, we made model predictions of expected spectra in order to assess how close we could come to this goal. The model had two components: quantitative absorption spectra, and estimates for mole fractions of species in decomposition gas. We made quantitative spectral models for CO_2, H2O, HCN, CH_4, H_2CO, N_2O, and CO, either by averaging HITRAN lines[3], or combining the NIST data base of qualitative spectra[5] with published band strengths. We also checked our work by sending a calibrated flow of CO_2 through a tubular fixture which held the fibers with a known gap. The observed spectra and the model agreed to within 30%. We estimated model mole fractions based on the decomposition species measurements made by mass spectrometry by the Litzinger[6-8] and Behrens[9-10] groups. They measured under different conditions, and got somewhat different values. Our choices mostly reflect the mole fractions published by the Litzinger group, and are: 18% H_2O, 13% HCN, 1% CH_4, 15% H_2CO, 6% CO_2, 5% N_2O, 5% CO and 22% NO. The resulting model spectrum is shown in Figure 7.

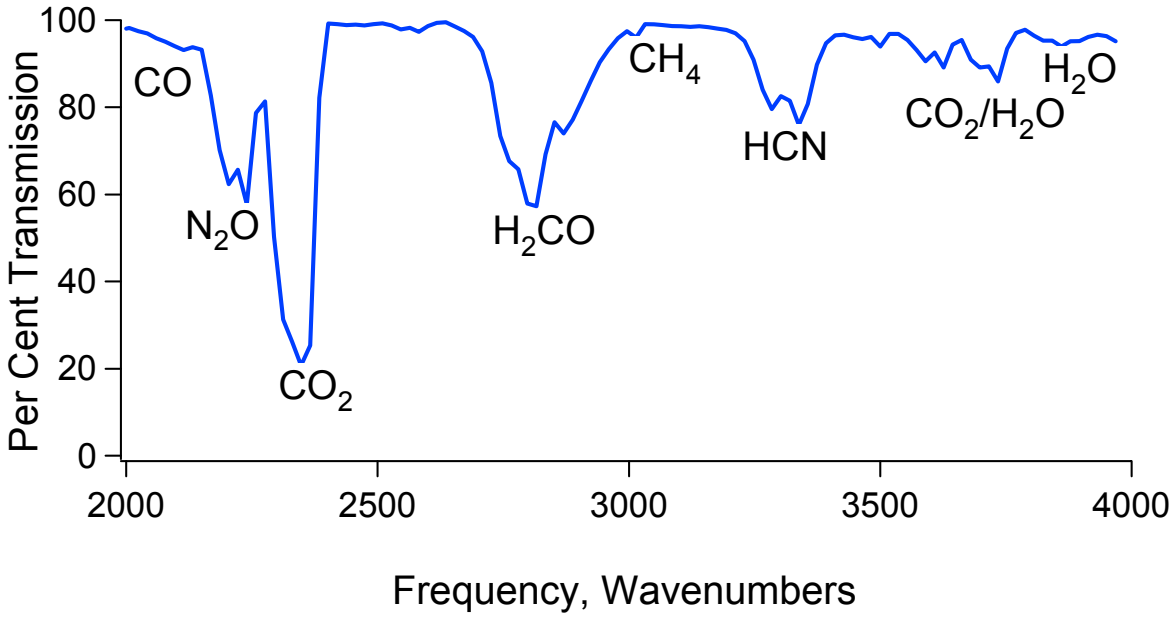

Figure 7. Predicted Model Spectrum for Pure Decomposition Gas at 6 atm with a 0.3 cm Absorption Path Length.

3.3 Individual Spectra

In our first round of strand burning work,[1] we inserted fibers by cutting the strand in half, pressing a groove in one face in which the fiber segments rested, and then gluing the two halves of the strand back together. We observed steady-state times, during which N_2O concentrations and infrared transmission remained roughly constant, in the range of 0.3 to 0.7 s. However, we had concerns that this insertion technique might be perturbing the burning process, perhaps slowing the burning rate through the fiber insertion region, so we changed to the current method of drilling holes the diameter of the stripped fiber. With this technique, steady-state times in the 0.03-0.04 s range were more typical,[2] and even the 0.01 time for N_2O measurement seen in Figure 3 was not the lower limit— some burns were carried out with no noticeable problems except that no N_2O was observed before transmission was lost.

Since the fastest data acquisition rate we achieved using the MIDAC FTIR spectrometer is 14 Hz (at its lowest resolution of 32 cm^{-1}, used by us in all burns), this suggests that we can often expect only one spectrum with substantial decomposition gas absorption features before transmission is lost, and at least sometimes we expect no good spectra at all. This was indeed our experience, as we now show using typical examples from an individual burn.

Figure 8 shows that transmission is lost while the flame front is far (0.1 cm) from the fiber/thermocouple plane, and only two spectra (276/277) are collected with any significant combustion gas features. We will examine these two spectra and their predecessor in the following three figures.

In Figure 9, spectrum 275, with only a tiny CO_2 feature, is noisier than the spectra that precede it. In particular, we think the feature at 2950 cm^{-1} is the Fourier transform of electronic pickup noise of the interferogram. In Figure 10 of spectrum 276, only CO_2 is observed at S/N better than 1. In Figure 11 of spectrum 277, CO_2 and N_2O are clearly seen, perhaps more than in the model. H_2CO detection is made difficult by neighboring noise. The match to the model HCN band might be compelling, if only the S/N for the spectral region to higher frequency (where our source intensity is lower) were not so bad. We concluded that only CO_2 and N_2O were certainly detected, but that averaging spectra might yield convincing H_2CO or HCN spectral features.

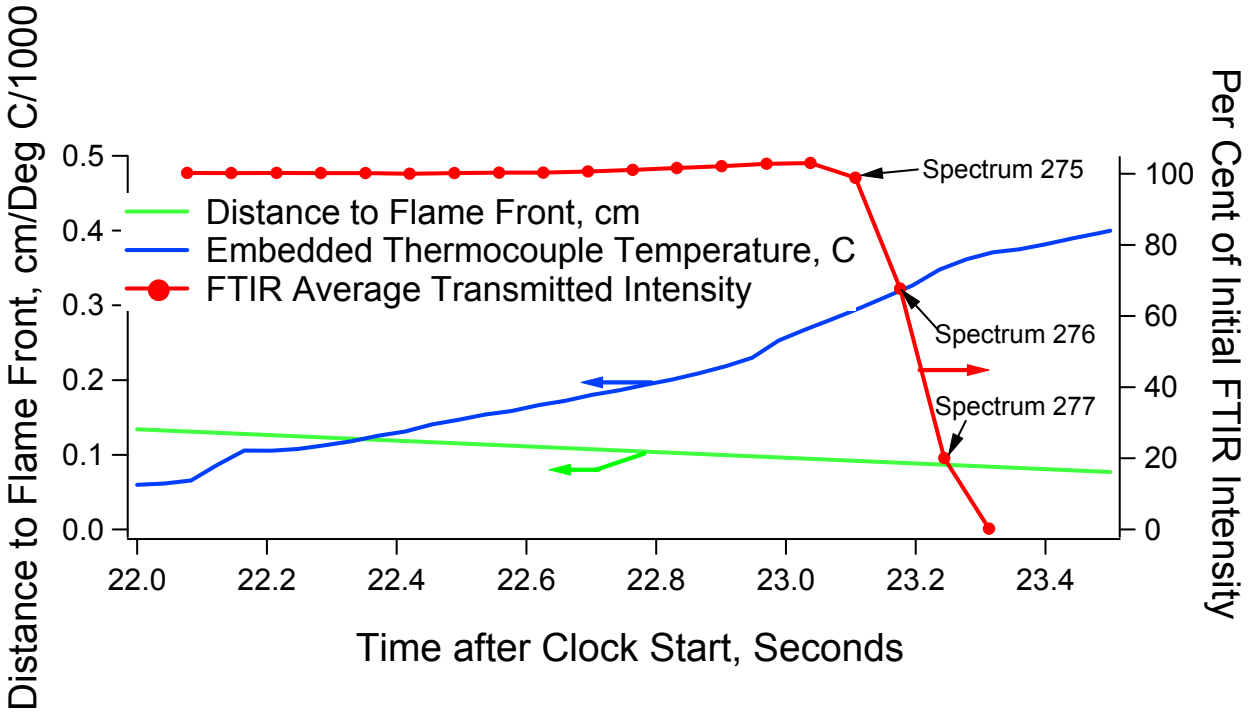

Figure 8. Transmitted Infrared Intensity (red curve), Flame Front Position with Respect to Fiber Insertion Plane (green curve) and Embedded Thermocouple Temperature in ºC/100 (blue curve) for Example Burn.

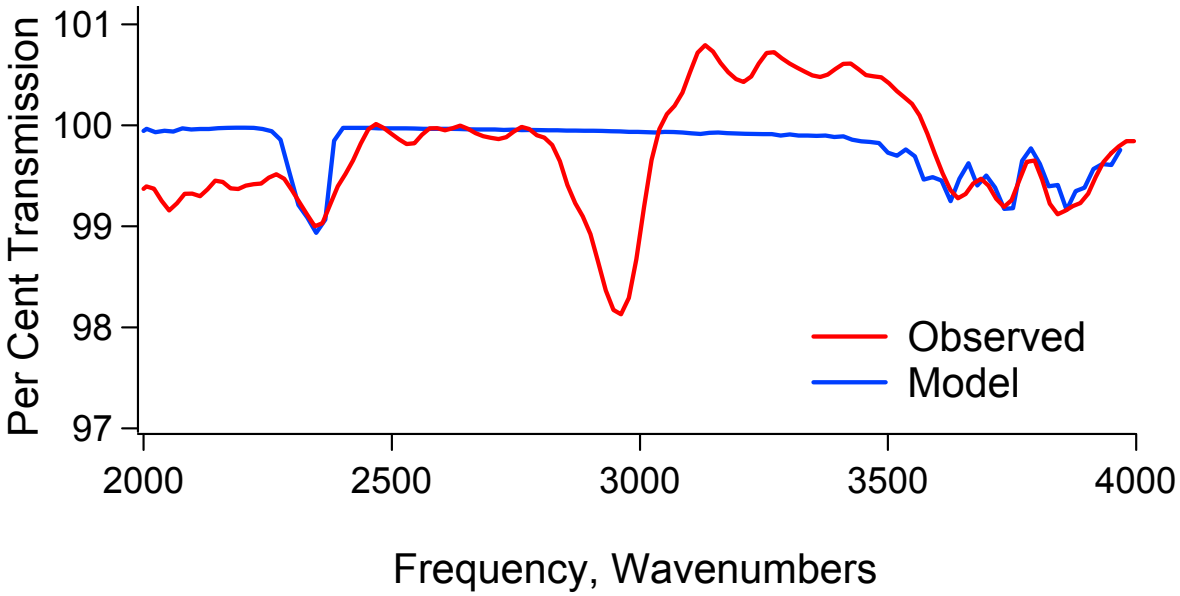

Figure 9. Spectrum 275 from the Burn History Shown in Figure 8. The Model Contains a CO_2 Mole Fraction of 0.04%, and an H_2O Mole Fraction (Only for Illustrative Purposes, Not Because We Believe It Is Present) of 3%.

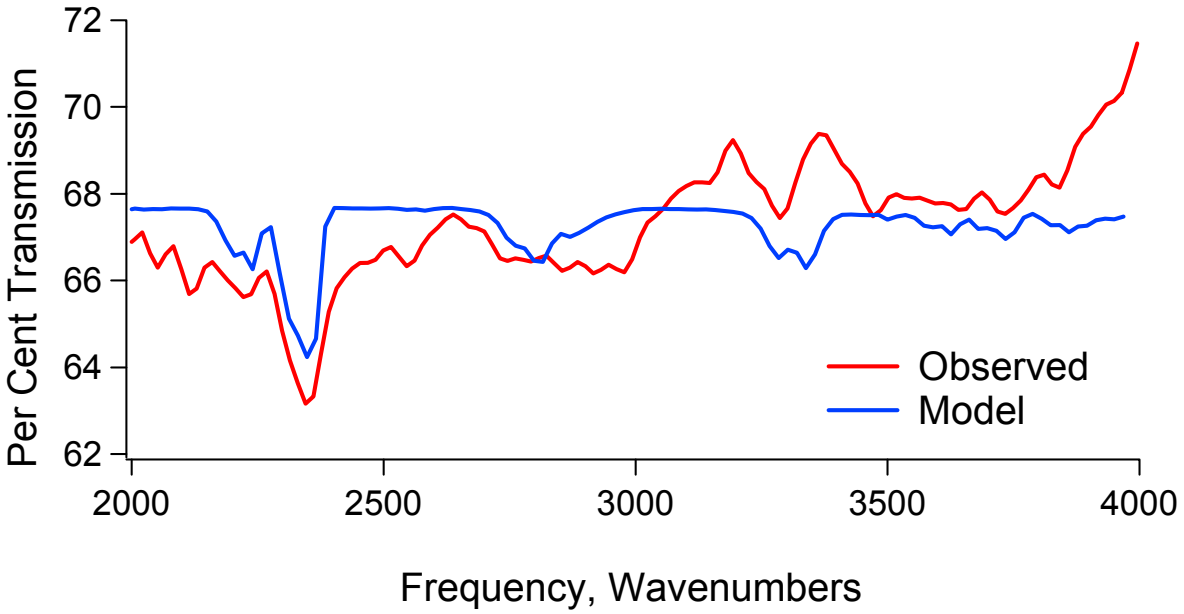

Figure 10. Spectrum 276 from the Burn History Shown in Figure 8. The Model Contains CO_2 and N_2O Mole Fractions of 0.2%, and (Only for Illustrative Purposes, Not Because We Believe They Are Clearly Present) an H_2CO Mole Fraction of 0.5%, an HCN Mole Fraction of 1% and an H_2O Mole Fraction of 3%.

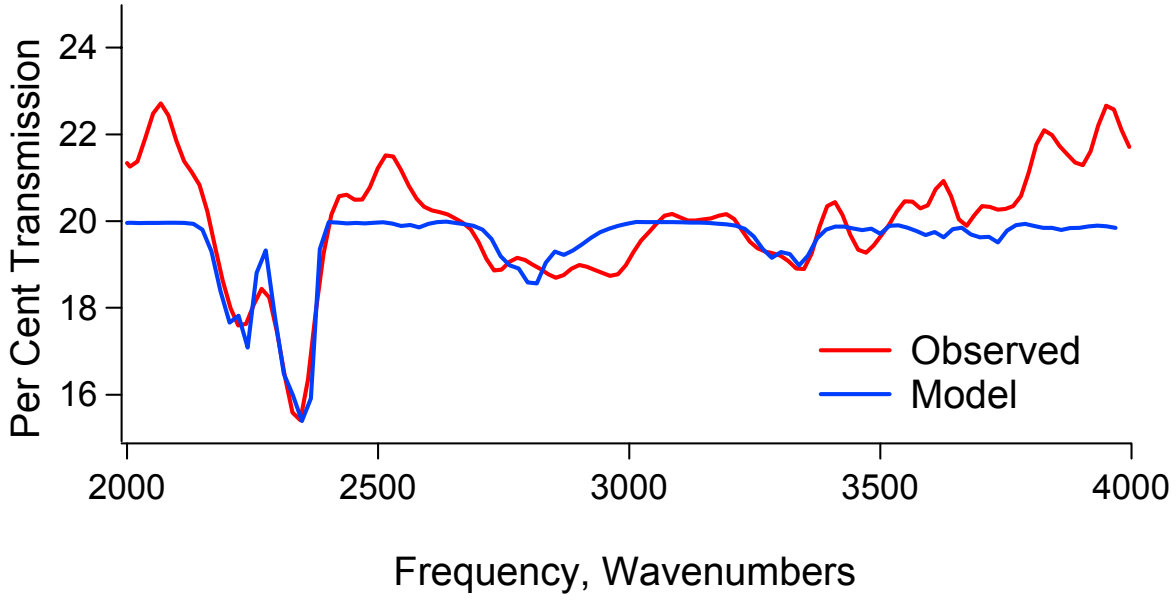

Figure 11. Spectrum 277 from the Burn History Shown in Figure 8. The Model Contains a CO_2 Mole Fraction of 1%, an N_2O Mole Fraction of 1.5%, and (Only for Illustrative Purposes, Not Because We Believe They Are Clearly Present) an H_2CO Mole Fraction of 0.5%, an HCN Mole Fraction of 1% and an H_2O Mole Fraction of 3%.

3.4 Results of Averaging Spectra

We found that the characteristics seen in the above examples applied to the data from all our successful burns. First, the S/N ratio was such that CO_2 and N_2O can usually be seen clearly, but detection of other species cannot be convincingly demonstrated. Second, the time during which a useful observation can be made was short, and there was typically only one spectrum in which transmission was substantially affected by the arrival of the flame front, but had not been driven to zero. This spectrum usually, though not always, showed strong CO_2 and N_2O absorption features, while weaker features were seen one or two spectra before it. Therefore, once we had accumulated data sets from a few burns, we investigated whether averaging the best spectra led to any clearer detection of additional molecular species. To introduce the spectra we used, we plot the time history of infrared transmission for 4 burns in Figure 12.

Figure 1 was generated by displacing the time records of four burns until the transmission loss times were superimposed. No decomposition gas absorption features are seen until the transmission through the fibers starts to drop, and then, as seen from the marker positions on the red curves, there are only a few spectra before transmission is lost completely. With pressed-groove fibers,[1] we can work back from tabulated distances to derive a time between N_2O appearance and transmission loss of 1.8 s, while in Figure 1 this time is at most twice the time between spectra, or about 0.15 s. The blue curve of distance to the flame front is at the center of a family of four curves for the specific burns, which all have the same slope (same burning rate) but different values at the transmission loss point. The total range of these distances is almost 0.4 to 1.4 mm, while the tabulated range for pressed-groove fibers[1] was 0 to 1.6 mm. The main point to be made is that this distance, and the somewhat larger distance at which decomposition gases are first seen, are both still of the order of 1 mm, a macroscopic distance.

Finally, the green curve of embedded thermocouple temperature is representative of the three burns done in January 2003, while the temperature curve for the June 2002 burn is much higher. This discrepancy may simply have to do with tilted flame fronts in the various experiments. The range of temperatures at transmission loss for pressed-groove fibers[1] was 50 to 330 ºC. The three 1/2003 burns had corresponding values even a bit lower than this range, while the 6/2002 temperature at transmission loss was about 350 ºC, just outside this range on the high side. The lesson to be drawn from these comparisons is that while burns continued to be highly variable, there is no evidence of systematic differences between the FTIR-observed burns of the present program and the earlier burns observed by other techniques, with the exception of the differences due to the method of fiber insertion.

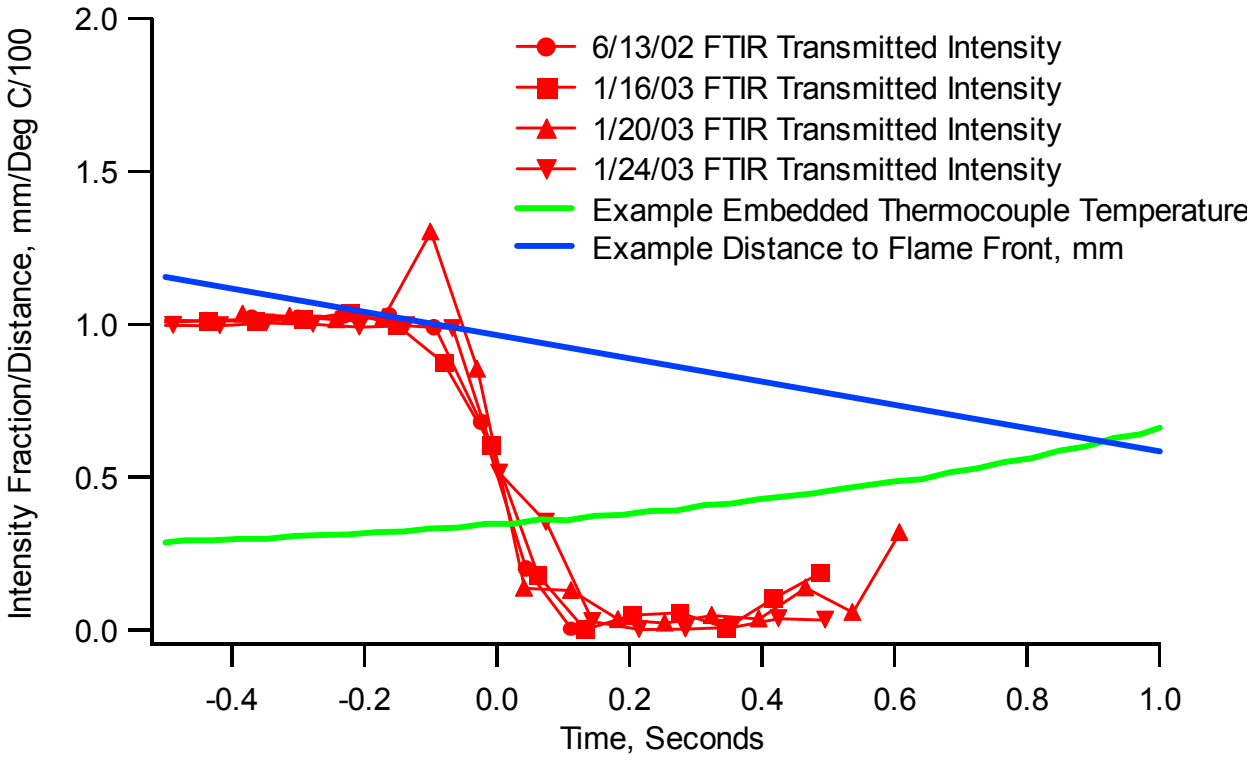

Figure 12. Example time dependent quantities from several recent burns. The red curves are infrared intensity transmitted through the fiber, with each symbol denoting a spectrum. The blue curve is the distance between the flame front and the fiber plane in mm— it is the average for the four burns, although the total range of such curves was 0.5 mm on either side. The green curve is the temperature of a thermocouple embedded at the fiber plane. This is once again a representative curve, but here it is the central one of three closely similar curves for the three 1/2003 burns— the 6/2002 burn temperature curve was much higher when transmission was lost.

The results of picking the one high-decomposition-gas-concentration spectrum from each burn and averaging them, for the four burns in Figure 12, are presented in two different ways in Figures 13 and 14. In Figure 13 the line weight of the red, observed spectrum changes proportionally to the number of spectra which contained each spectral feature. So, for example, all four spectra showed a CO_2 band, while 3 out of 4 clearly showed an N_2O band. The fourth, the purple dotted curve in Figure 14, may have N_2O as a shoulder. The shape of the spectrum in that region turns out to be a very good match to the CO band, although the size of the two peaks that give that impression is really at the noise level of the observation. The feature at 2000 cm^{-1}, seen at some level in all spectra though most strongly in one, corresponds to neither CO, to its right, or NO, seen on its left in Figure 14. With no further evidence, we take it to be a noise feature, not a real absorption band.

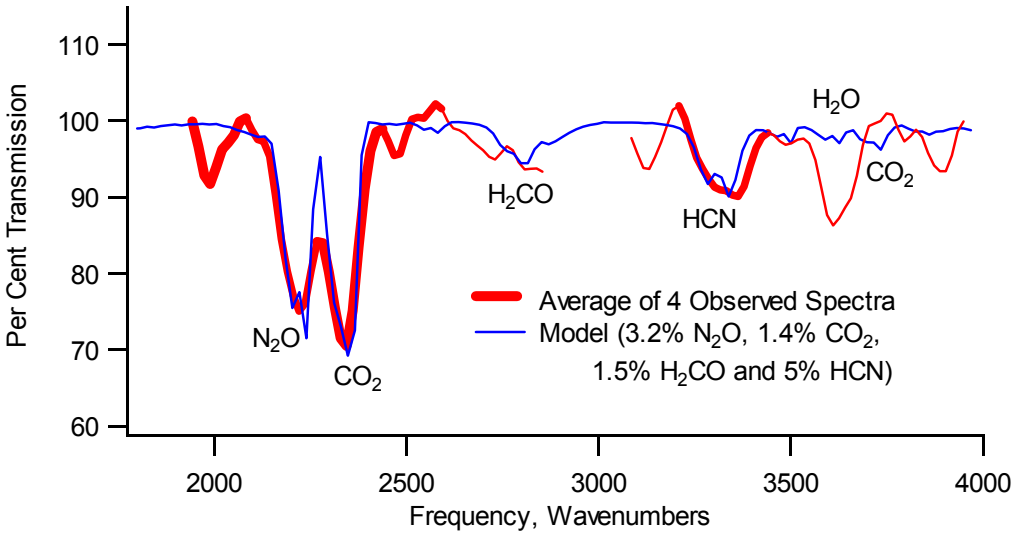

Figure 13. Average of observed spectra compared to approximate fit to model bands. In the observed curve, the line weight is proportional to the number of spectra exhibiting each feature.

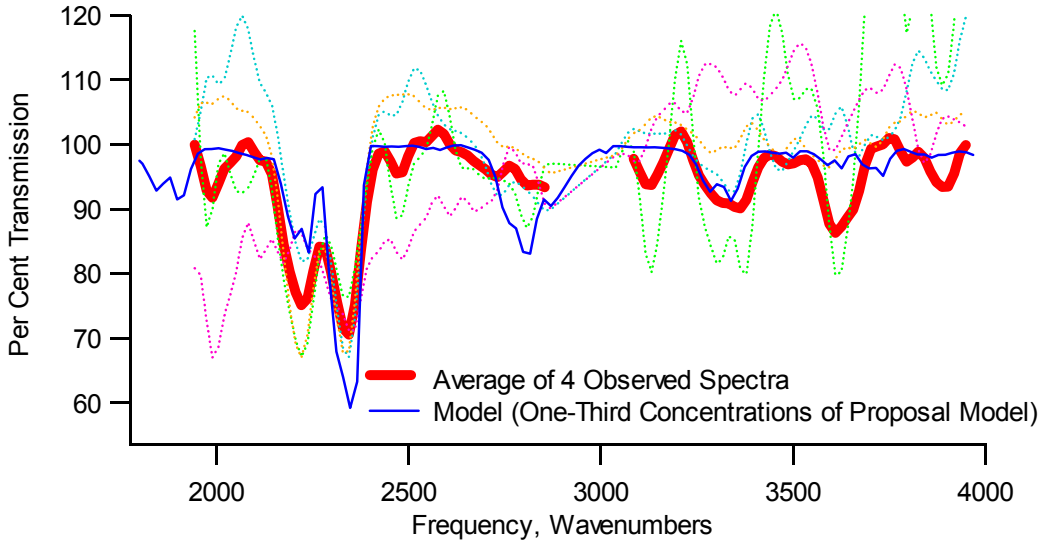

Figure 14. Average of observed spectra compared to scaled version of model of Figure 7. The four individual spectra used are presented in the dotted curves.

After the CO_2 and N_2O bands, the best match between model and observation is the HCN band. However, in this case the majority of the contribution to the average comes from only one of the four spectra, and it is the same spectrum which also contributes the two similarly-sized features on either side of it. These do not match with any molecular absorption spectra we know, and so for now we take them as noise features also. This leaves the reality of the HCN feature in doubt, however plausible it looks in the averaged spectrum.

In Figures 13 and 14, we have omitted plotting the observed spectra in a range around 3000 cm^{-1}. This spectral region continues to be plagued by additional noise, which we attribute to interference from 60 Hz (or harmonics) pickup. This is unfortunate because it overlaps with the position of the formaldehyde absorption band. The match in shape between averaged observations and model is much less compelling than for HCN, though some of that could be due to the influence of the neighboring high noise region.

The model curve in Figure 13 has the individual band intensities adjusted to roughly match the observed features to which they may correspond. This Figure 13 model has no contribution from NO, CO, or water (the region at the right-hand side of the spectrum which has contributions from both CO_2 and H_2O also has lower blackbody signal and higher noise— even very large water concentrations would not be easily seen). Figure 14, on the other hand, uses a model curve based on the one we developed for the proposal (Figure 7). The concentrations in this model were based on mass spectroscopic analyses of pure decomposition gas. The model in Figure 14 divides all of those concentrations by a factor of 3, which brings most spectral features into factor-of-two agreement. This suggests that the model in Figure 13 could be consistent with a spectrum of diluted decomposition gas, but by no means proves it.

In the above discussion we have identified two problems: the short observation time, and the low signal-to-noise ratio of the spectra. We found no better solution to the latter problem than taking more spectra to contribute to an average spectrum with lower noise. We had hoped to try dealing with the former problem by borrowing or renting a faster FTIR spectrometer, but after discussions with operators of two instruments we conclude that the throughput of fast FTIR spectrometers is so much lower that they are unusable.

4. Our Results in the Context of a Model of Condensed Phase Processes

The key issues for understanding nitramine propellant combustion have remained much the same over the last decade. In an extensive review undertaken by the JANNAF Panel on Kinetic and Related Aspects of Propellant Combustion Chemistry, a one and a half day workshop held in conjunction with the 31st JANNAF Combustion Meeting in 1994, Richard Behrens identified key components of a condensed phase model including the "amount and partitioning of heat generation in condensed phases and the identity and rate of release of lower molecular weight species into the gas phase." It was pointed out that although these species are largely the same as the set known from gas phase modeling and diagnostics, mole fractions in subsurface decomposition may differ greatly from those in the gas phase. He also noted that modeling of the above processes was "in its infancy, due to tight coupling of processes and lack of diagnostics that can probe these processes directly." And in his 1995 report for the same panel, chairman Prof. Merrill Beckstead gave as his examples of items still to be addressed before a reliable model of condensed phase processes can be constructed "determining how the reaction pathways change as a function of temperature and heating rate, and quantifying the role of bubbles in the condensed phase process."

In a 1996 report on an Army workshop, Martin Miller of ARL had occasion to review the state of the art in solid propellant combustion modeling.[11] He pointed out that the RDX modeling work of the Pennsylvania State University group carried out under the University Research Initiative from ARO had "broken new ground in describing the two-phase subsurface reaction zone...in a one-dimensional formalism using the concept of microscopic porosity, gas from subsurface RDX decomposition and evaporation being assumed to account for void formation and growth." He also noted the "only the Penn State code has exercised [its] capability for any number of condensed phase reactions". On the other hand, in reviewing the approximations made in current models, he reports "in the condensed phase there is some concern about the present use of global reactions for RDX. This type of description has proven to be hazardous in the gas phase; there is no reason to believe it will be less so in the condensed phase...There is an urgent need to develop fundamental theoretical models of the chemistry and physics of the condensed phase as well as experimental tools for characterizing the subsurface region. A related concern is the validity of the porosity concept for describing the complex three-dimensional foam zone."

More recently, the Penn State group has gone beyond their RDX modeling work to apply their model to mixtures of the ingredients of the current Army nitramine gun propellants including XM39.[12] Miller at ARL is also developing modeling capabilities which will be important components of an advanced three-phase combustion code which will eventually be applied to nitramine propellants. The Brewster group at the University of Illinois, in work for the Office of Naval Research and Los Alamos National Laboratory, is also developing a nitramine combustion model with global chemistry in both gas and condensed phases.[13] Models with detailed gas-phase

chemistry and one or more condensed phase reactions have been presented by Melius,[14] Beckstead,[15] and Prasad, Yetter and Smooke.[16]

In summary, modelers are now coming to grips with the details of propellant combustion processes in condensed phases. However, as pointed out by Ermolin and Zarko in their 1998 review,[17] condensed phase models are not first-principles models. Instead, "the description of condensed-phase processes has been implemented at a very approximate level, and… the choice of global reactions and kinetic parameters does not have a reliable basis." In a review focusing on *modeling* of nitramine combustion, they conclude by saying, "The need to develop new experimental approaches to studying the structure and dynamic behavior of the combustion wave retains its importance. In particular, it remains unknown how a two-phase medium is formed in a liquid layer, how gas is liberated from a condensed substance, and what conditions characterize processes on a burning surface."

The data presented in this report suggest that a program of phenomenological analysis aimed at confirming or disproving our explanations of what we observe could be profitable. Questions which could be asked in such a program include the following: Given estimates of thermal expansion parameters for the components of a composite propellant, and the characteristics of the thermal wave, what can be said about the tendency of the propellant to form cracks? Given evolution rates of RDX decomposition products from the work of Behrens and others, as well as RDX evaporation rates, what can be said about the formation of pressurized voids in a region where RDX has begun to melt but the propellant retains some structural integrity? How high could the pressure go, and how big would the total volume of voids have to be compared to the observation volume between the two fibers? Given reasonable surface and gas-phase reaction rates, is it reasonable that reaction of NO_2 in the observation volume might reduce its concentration in a time scale of order 1 second? Or is dilution by decomposition gases from a different regime a better explanation? All of these questions and more could be addressed in a simple, order-of-magnitude fashion. In some cases, the answer will be clear even allowing for large uncertainties associated with both inputs and calculational methods. In other cases, the results might suggest improving those input parameters, perhaps through laboratory experiments, or upgrading the calculational methods.

Finally, we should add that there is also additional work to be done in making clear the connections between our work and the observations of other experimental groups. In this regard, we take particular note of the recent work by Behrens and co-workers[10,18-19] in which both chemical and physical measurements, the former using his well-developed mass spectrometric techniques, the latter involving quenching of the decomposition process at various stages, followed by scanning electron microscopy (SEM). These investigations of HMX and RDX showed some of the physical characteristics, such as cracking and bubble formation, that have been observed by

other SEM studies, but put them in the context of what gaseous decomposition products are being evolved during their formation. As this work progresses, it should provide very complementary information to the types of chemical and physical observations we made.

5. Summary

Simultaneous records of infrared and visible absorption as well as video and embedded thermocouple data, all recorded at data rates of at least 10 Hz, have allowed us to put together a picture of the physical and chemical processes in a very specific region: that layer of a burning composite propellant which is hot enough to result in significant decomposition chemistry, but below the temperature at which all components dissolve into a liquid layer. At least in the XM39 propellant we studied, we believe our observations are due to the formation of pressurized bubbles of decomposition gas in regions near the flame front, coupled with the formation of cracks extending distances of 0.1 cm into the cooler propellant. These cracks may arise from differential thermal expansion, or preferential loss of one or more propellant components. A key feature of this hypothesis is that the propellant binder remains structurally sound enough to support the pressure differential that can cause sudden appearance of decomposition gas when a crack opens up, even as the RDX in the binder matrix reaches temperatures that allow its rapid decomposition. The next step in this investigation should be an analysis, at an engineering level, of this hypothesis in terms of known or newly measured properties of the propellant components.

6. Publications and Technical Reports Supported Under This Contract

(a) Papers published in peer-reviewed journals

None.

(b) Papers published in non-peer-reviewed journals or in conference proceedings

None.

(c) Papers presented at meetings, but not published in conference proceedings

"Spectrally Analyzed Embedded Infrared Fiber Optic Diagnostic of Advanced Composite Propellant Combustion", J. Wormhoudt, poster presented at the 2002 Gordon Conference on Energetic Materials.

(d) Manuscripts submitted, but not published

None.

(e) Technical reports submitted to ARO

"Spectrally Analyzed Embedded Infrared Fiber Optic Diagnostic of Advanced Composite Propellant Combustion", J. Wormhoudt, ARI-LR-38, Interim Progress Report for 2000, March 2001.

"Spectrally Analyzed Embedded Infrared Fiber Optic Diagnostic of Advanced Composite Propellant Combustion", J. Wormhoudt, ARI-LR-39, Interim Progress Report for 2001, March 2002.

"Spectrally Analyzed Embedded Infrared Fiber Optic Diagnostic of Advanced Composite Propellant Combustion", J. Wormhoudt, ARI-LR-40, Interim Progress Report for 2002, March 2003.

7. Participating Scientific Personnel

Dr. Joda Wormhoudt, Aerodyne Research.

Dr. Roger Putnam, Aerodyne Research.

Dr. Kurt Annen, Aerodyne Research.

Dr. David Nelson, Aerodyne Research.

Dr. J. Barry McManus, Aerodyne Research.

Dr. Charles E. Kolb, Aerodyne Research.

Shannon Dong, undergraduate, MIT Department of Aeronautics and Astronautics

No advanced degrees were earned by personnel employed on the project.

8. Report of Inventions

No inventions were associated with this project.

9. References

1. J. Wormhoudt, P. L. Kebabian, and C. E. Kolb, "Infrared Fiber Optic Diagnostic Observations of Solid Propellant Combustion", Combustion and Flame 108, 42 (1996).

2. J. Wormhoudt, P. L. Kebabian, and C. E. Kolb, "Embedded Infrared Fiber Optic Absorption Studies of Nitramine Propellant Strand Burning", Combustion and Flame 111, 73 (1996).

3. L. S. Rothman, R. R. Gamache, R. H. Tipping, C. P. Rinsland, M. A. H. Smith, D. C. Benner,V. Malathy Devi, J.-M. Flaud, C. Camy-Peyret, A. Perrin, A. Goldman, S. T. Massie, L. R. Brown and R. A. Toth, J. Quant. Spectrosc. Radiat. Transfer 48, 469 (1992).

3. R. Klein, M. Mentser, G. Von Elbe and B. Lewis, J. Phys. and Colloid Chem. 54, 877 (1950).

4. S. E. Stein, C. Clifton, J. Gallagher, A. Shamim and H. Zohdi, NIST Standard Reference Database Series 35: The NIST/EPA Gas Phase Infrared Database, National Institute of Standards and Technology, 1992.

6. B.L. Fetherolf, and T.A. Litzinger, "Chemical Structure of the Gas Phase Above Deflagrating RDX: Comparison of Experimental Measurements and Model Predictions," Proceedings of the 30th JANNAF Combustion Subcommittee Meeting, CPIA Publication No. 606, Vol. II, p. 15, (1993).

7. B.L. Fetherolf, T.A. Litzinger, Y.-C. Liu, and K. K. Kuo, "A Comparison of the Physical and Chemical Processes Governing the CO_2 Laser-Induced Pyrolysis and Deflagration of XM39 and M43," Proceedings of the 30th JANNAF Combustion Subcommittee Meeting, CPIA Publication No. 606, Vol. II, p. 183, (1993).

8. Y. Lee, C.-J. Tang, and T. A Litzinger, "A Study of the Chemical and Physical Processes Governing CO_2 Laser-Induced Pyrolysis and Combustion of RDX," Combustion and Flame 117, 600 (1999).

9. R. Behrens, Jr. and S. Bulusu, "Thermal Decomposition of Energetic Materials. 3. Temporal Behaviors of the Rates of Formation of the Gaseous Pyrolysis Products from Condensed-Phase Decomposition of 1,3,5-Trinitrohexahydro-*s*-triazine," J. Phys. Chem. 96, 8877 (1992).

10. R. Behrens, S. Mack and J. Wood, "Thermal Decomposition Mechanisms of HMX: The Interrelationship of Chemical and Physical Processes," paper presented at the JANNAF Combustion and Hazards Meeting, Tucson, AR, December, 1998.

11. R. W. Shaw, D. M. Mann and M. S. Miller, U. S. Army Workshop on Solid-Propellant Ignition and Combustion Modeling, 9-10, April 1996, Report ARL-TR-141, Army Research Laboratory, Aberdeen, MD.

12. Y.-C. Liau, V. Yang and S. T. Thynell, "Modeling of RDX/GAP Propellant Combustion with Detailed Chemical Kinetics," paper presented at the JANNAF Combustion and Hazards Meeting, Cocoa Beach, FL, October, 1999.

13. M. J. Ward, S. F. Son and M. Q. Brewster, "Steady Deflagration of HMX with Simple Kinetics: A Gas Phase Chain Reaction Model," Combustion and Flame 114, 556 (1998).

14. C.F. Melius, "The Thermochemistry and Reaction Pathways of Energetic Material Decomposition and Combustion," Phil. Trans. R. Soc. Lond. A 339, 365 (1992).

15. J. E. Davidson and M. W. Beckstead, "A Three-Phase Model of HMX Combustion," 26th Symposium (Intl.) on Combustion, The Combustion Institute, 1996, p. 1989.

16. K. Prasad, R. A. Yetter and M. D. Smooke, "An Eigenvalue Method for Computing the Burning Rates of HMX Propellants," Combustion and Flame 115, 406 (1998).

17. N. E. Ermolin and V. E. Zarko, "Modeling of Cyclic-Nitramine Combustion," Combustion, Explosion, and Shock Waves, 34, 485 (1998).

18. R. Behrens, "Thermal Decomposition of HMX: Morphological and Chemical Changes Induced at Slow Decomposition Rates", paper presented at 12th International Detonation Symposium, San Diego, CA, August 2002.

19. R. Behrens and S. Maharrey, "Chemical and Physical Processes that Control the Thermal Decomposition of RDX and HMX", in *Combustion of Energetic Materials*, ed. K. Kuo and L. T. DeLuca, Begell House, New York, 2002, pp. 3-21.